J. Phys. G: Nucl. Phys. **8** (1982) 13–32. Printed in Great Britain

Kaon scattering and charged sigma hyperon production in K^-p interactions below 300 MeV/*c*

J Ciborowski†, J Gwizdz†, D Kielczewska†, R J Nowak†, E Rondio†, J A Zakrzewski†, M Goossens‡¶, G Wilquet‡*, N H Bedford§**, D Evans§, G P Fleming§, Y A Hamam§, J V Major§, J H Bartley||, D H Davis||, D J Miller||, D N Tovee|| and T Tymieniecka|| +

† Instytut Fizyki Doswiadczalnej, Uniwersytet Warszawski, Poland
‡ Inter-University Institute for High Energies, (ULB–VUB) Brussels, Belgium
§ Department of Physics, University of Durham, Durham, UK
|| Department of Physics and Astronomy, University College, London, UK

Received 15 July 1981

Abstract. In an experiment on K^-–proton interactions in a hydrogen bubble chamber, the cross sections and angular distributions have been studied for elastic and charge-exchange scattering, and charged sigma hyperon production in the momentum range 90–300 MeV/*c*. Good agreement is found with previous cross sections except for the charge-exchange channel where the new values are 60% larger. The production distributions of the charged sigma hyperons and the polarisation of the Σ^+ hyperon clearly indicate that P waves are present down to about 150 MeV/*c*, much lower than previously reported.

1. Introduction

Although beams of negative kaons have been available since the early 1950s, many unresolved questions remain concerning their low-energy interactions. This is partly due to the production of low-energy short-lived hyperons which decay in distances of the order of a few millimetres and can be recognised only by visual techniques. The resulting low rate of data accumulation compared with counter methods, when combined with the variety of reaction channels, implies that considerable time is required to gather significant statistics in any one channel. This is reflected in earlier work (Nordin 1961, Humphrey and Ross 1962, Watson *et al* 1963, Abrams and Sechi-Zorn 1965, Sakitt *et al* 1965, Kim 1965, 1966, Schlosser *et al* 1965, Kittel *et al* 1977) where only two experiments examine all of the six reaction channels which are open near to the K^-p threshold, that is:

$$K^-p \rightarrow K^-p \tag{1}$$

$$\rightarrow \bar{K}^0 n \tag{2}$$

$$\rightarrow \pi^- \Sigma^+ \tag{3}$$

¶ Now at EP Division, CERN, Geneva, Switzerland.
* Chercheur Qualifié FNRS, Brussels, Belgium.
** Now at GEC Reactor Engineering Ltd, Whetstone, UK.
\+ Now at Instytut Fizyki Doswiadczalnej, Uniwersytet Warszawski, Poland.

0305-4616/82/010013 + 20$02.00

$$\rightarrow \pi^+ \Sigma^- \tag{4}$$

$$\rightarrow \pi^0 \Sigma^0 \tag{5}$$

$$\rightarrow \pi^0 \Lambda. \tag{6}$$

In the first of these two experiments, Watson *et al* (1963) concentrated on primary momenta in the region of 250–513 MeV/*c* and out of this was developed the detailed work of the LBL group (Mast *et al* 1968, 1973a, b, 1976a, b, Bangerter *et al* 1981) centred on the region about 390 MeV/*c* where the $\Lambda(1520)$ is maximally excited. Complementary to the work of Watson *et al* (1963) is that of Kim (1966) where a comprehensive coverage of the reaction channels was attempted in the region of 80–300 MeV/*c*, although with limited statistics. This latter experiment has been important in extrapolations to negative energies in kaon–nucleus interactions (Henley *et al* 1980), in determining the kaon–nucleon–hyperon coupling constants and in analysis based on forward dispersion relations (Martin 1981). In some of these analyses the reliability of parts of this earlier experiment (Kim 1966) has been questioned (Davis *et al* 1977, Miller 1980). A more serious difference is seen in comparisons of scattering lengths derived from interactions of K^- mesons at rest and in flight with those derived from the locations and widths of x-ray lines of kaonic atoms (Batty 1980).

However, it should be pointed out that analysis of these data in terms of a *K* matrix (Kim 1967) leads, by extrapolation below threshold, to a $\Lambda(1405)$ whose mass value is quite consistent with that found by production experiments (Chao and Kraemer 1973). One of the aims of low-energy experiments has been to determine the dynamical nature of the $\Lambda(1405)$, but so far this has not been achieved (Martin 1981, Dalitz and McGinley 1981, Kumar 1981).

At low momentum it is usually assumed that S waves only are present and all *K*-matrix analyses are based on this precept. At 390 MeV/*c* where the $\Lambda(1520)$ is produced, D waves are very strong. Although P waves are expected at lower momenta the earlier experiments suggested that these are of little importance below 280 MeV/*c*. Obviously the onset and size of the P-wave contribution is crucial to determining the range and validity of the usual S-wave, *K*-matrix analyses.

In this paper and subsequent reports new data on the reaction channels at low momenta will be presented and analysed. Different methods of analysis are required in different channels. For example events in channels (5) and (6) are topologically ambiguous and the overall classification of these events requires a detailed analysis by techniques of missing mass and of Monte-Carlo simulation. This paper is devoted to the presentation and analysis of new data from channels (1)–(4) in which the events are usually unambiguously identified, that is, elastic and charge-exchange scattering and charged Σ hyperon production. Although the general features of the new data are largely in agreement with those of earlier experiments there are significant differences.

2. The exposure and experimental conditions

The exposures were carried out with the 1.5 m British National Hydrogen Bubble Chamber which had been modified by the inclusion of a track sensitive target of hydrogen liquid (TST). From the NIMROD accelerator at the Rutherford Laboratory, a 620 MeV/*c* negative kaon beam was transported to the chamber. There it was degraded in momentum

to about 250 MeV/c by a block of aluminium placed inside the chamber†. At this momentum most of the kaons emerging from the degrader stopped inside the hydrogen (which was at a density of 0.0566 g cm^{-3}). The TST, which extended down the whole length of the chamber, was 8 cm × 44 cm transverse to the beam and outside this the rest of the chamber was filled with a hydrogen–neon mixture (~70–80 molar per cent neon). This gave enhanced conversion of γ rays to electron pairs with a radiation length of about 45 cm compared with that of hydrogen which is about 10 m. The use of converted γ-ray information has been confined largely to the Σ^0 and Λ^0 channels.

Although the shallow TST introduced geometric problems, a compensating feature was that the running conditions of the composite chamber led to small-sized bubbles in the hydrogen and consequently to an improved resolution of the separation of nearby vertices. This has already been used to advantage in a study of the production of neutral and charged hyperons at rest (Nowak *et al* 1978, Goosens *et al* 1981).

2.1. *Scanning, measuring and processing of events*

Films have been scanned for events which could belong to channels (1)–(6) for kaons in flight. All production and decay vertices were required to be in hydrogen. Although the majority of primary kaons (~85%) came to rest before interacting there is little contamination by them of the 'in-flight' events in channels (3) and (4) since the Σ channels are exothermic and the events in flight are clearly distinguished from those at rest by the non-collinearity of the tracks of the Σ hyperon and the pion. Channels (1) and (2) are absent for kaons interacting at rest. The 'at rest' events are made use of in track length normalisation for cross section determinations (see below). Also for purposes of normalisation some of the films have been scanned for samples of one- and three-prong events due to the decays of the kaons.

Events have been measured and processed through the Rutherford Laboratory chain of programs, GEOMETRY and KINEMATICS. A proportion of events remaining unsuccessfully measured after three measuring attempts has been allowed for in determining cross sections.

2.2. *Selection of events for analysis*

Before analysis all events were subjected to a set of selection criteria which put limits on geometric variables so that within these limits there is a negligible loss of events due to short, steep or unmeasurable tracks. Corrections were then made for the excluded and lost events. The particular cuts made to each channel and their effects are discussed below in the channel-by-channel presentation of the analysis.

In order to reduce the problems associated with the geometry of the TST all production and decay vertices had to be found within a fiducial volume where vertices were required to be further than 2 mm from each vertical TST wall.

Both charge-exchange and the hyperon channels involve production and decay vertices. By examining the mean lifetime of the decaying particle as a function of the separation, r_s, of the vertices, a range of separations can be specified within which losses and ambiguities are insignificant. The minimum value of this separation depends on whether the particle connecting the vertices is charged or neutral. Events with r_s outside the specified range are cut from the sample. The visibility of events depends upon the

† Exposures to higher momentum were also made (Fallahi 1977, Hamam 1978).

angles of scattering, production and decay as seen in the chamber. That losses exist has been established by forming the distributions of centre-of-mass angles of decay, $\cos\theta_d^*$, and of the angles, φ, where for the production and decay vertices respectively

$$\cos\varphi_p = (\boldsymbol{K}\times\boldsymbol{Z})\cdot(\boldsymbol{K}\times\boldsymbol{P})/|\boldsymbol{K}\times\boldsymbol{Z}||\boldsymbol{K}\times\boldsymbol{P}|$$

$$\cos\varphi_d = (\boldsymbol{P}\times\boldsymbol{Z})\cdot(\boldsymbol{P}\times\boldsymbol{D})/|\boldsymbol{P}\times\boldsymbol{Z}||\boldsymbol{P}\times\boldsymbol{D}|.$$

Here the vectors represent the directions of the kaon ($\boldsymbol{K}$), the optical axis of the chamber ($\boldsymbol{Z}$), the produced particle ($\boldsymbol{P}$) and the decay particle ($\boldsymbol{D}$). The angle φ is 'folded' into a range of 0–90°. All these distributions should be isotropic and cuts have been made to exclude from the sample those events which lie in those parts of the distributions obviously depleted by scanning losses. The losses associated with the centre-of-mass scattering or production angle ($\cos\theta_p^*$) are considered separately for each channel (see below).

2.3. Normalisation of events for cross section determinations

The beam comprised a wide spectrum of energies. This together with its rapid energy loss along the chamber and a contamination of about 20% from other negative particles creates a difficulty in determining directly the length of beam track per momentum interval and consequently the cross sections. Two methods have been adopted, each of which is preferred in its own energy regime.

The first of these is based on the 'one-prong', i.e., one charged particle, modes of kaon decay seen in the fiducial volume of the chamber. The number of these per momentum bin leads directly to an estimate of primary track length. The numbers of events due to strong and decay interactions are classified by measured rather than by fitted momentum. The reasons for this are given in the appendix where the use of the mean fitted momentum of three-pion decays as a 'plotting momentum' is also discussed. The plotting momentum is a means of correcting for any small systematic differences between measured and true momentum.

The second method is peculiar to low-energy kaon experiments. It uses those events in which the primary kaon has stopped, or would have stopped ('WHS' method) but for an interaction in flight, in the fiducial volume of the chamber. Working upstream from the stopping points the distribution of track lengths within each momentum interval can be determined (details are to be found in the appendix). In this normalisation primary events are classified according to fitted momentum. This method is particularly useful for primary momenta $\leqslant$170 MeV/c, whereas the first is more appropriate to momenta above 150 MeV/c. The track lengths deduced from these methods will be presented later.

3. Elastic scattering

The TST technique combined with low energies sets limitations to the study of elastic scattering. Firstly at low primary momentum the recoiling proton may not lead to a visible track and the process then appears merely as a kinked kaon track. Secondly it is known that a small quantity of neon diffused into the hydrogen TST. By studying K^- interactions at rest it has been established that this contamination makes a negligible contribution to the inelastic channels since very few events are seen with charge imbalance. However, neon nuclei present a much higher Coulomb scattering cross section than those of hydrogen and the track of the recoiling massive neon nucleus is always invisible. Consequently

scatterings without recoil are of doubtful origin and cannot readily be used in the analysis. These discarded events correspond to a range of scattering angles in which interference between the nuclear and Coulomb scatterings in hydrogen occurs. Hence this region of interference cannot be reached in the present experiment and so the observed scattering angular distributions should be isotropic unless other than S waves are involved. Also at low energy, despite the available track length after a scatter being small, there is a substantial probability of elastic scatterings being followed by a secondary interaction. These events are difficult to measure successfully but unless they are included a momentum bias would be introduced on the cross section determination.

In total 2233 events were found and classified as elastic scatters with an overall scanning efficiency of 99.3%. Satisfactory measurements were made of 2073 events of which 1815 were successfully fitted to elastic scatterings. These were subjected to the same criteria on vertex coordinates as were applied to the selection of one-prong kaon decays which were used to estimate the primary kaon path length. Finally a total of 1691 fitted events remained for detailed analysis.

After the scatter many kaon and proton tracks of less than 1 mm are lost so momentum-dependent biases are present. This may be seen by reference to figure 1 where the kinematics of elastic scattering are presented. The loss should be very severe in the lowest range of primary momentum considered, that is 110–150 MeV/c, and it should become relatively small at the highest interval of 230–300 MeV/c. Such an effect is apparent in the CM angular distributions of figure 2. There is also a loss of events whose planes of scattering lie approximately normal to the scanning plane of the chamber as seen in the distribution of the angle φ.

The cuts which have been adopted, the number of events thus selected and the scaling

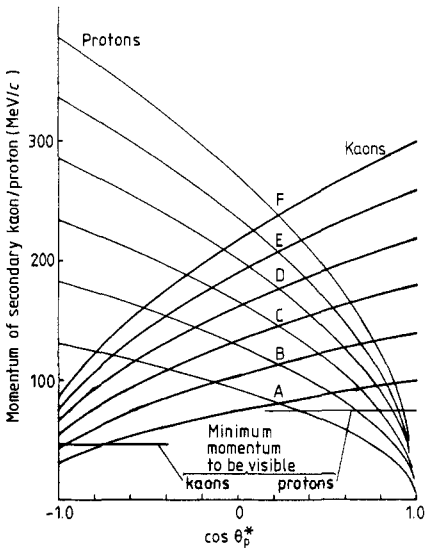

Figure 1. Kinematics of elastic scattering. Momenta of secondary particles are given as a function of production angle and primary momentum. At 100 MeV/c, both secondaries are visible only for $-0.75 < \cos\theta_p^* < 0.35$. Primary momentum (MeV/$c$): A, 100; B, 140; C, 180; D, 220; E, 260; F, 300.

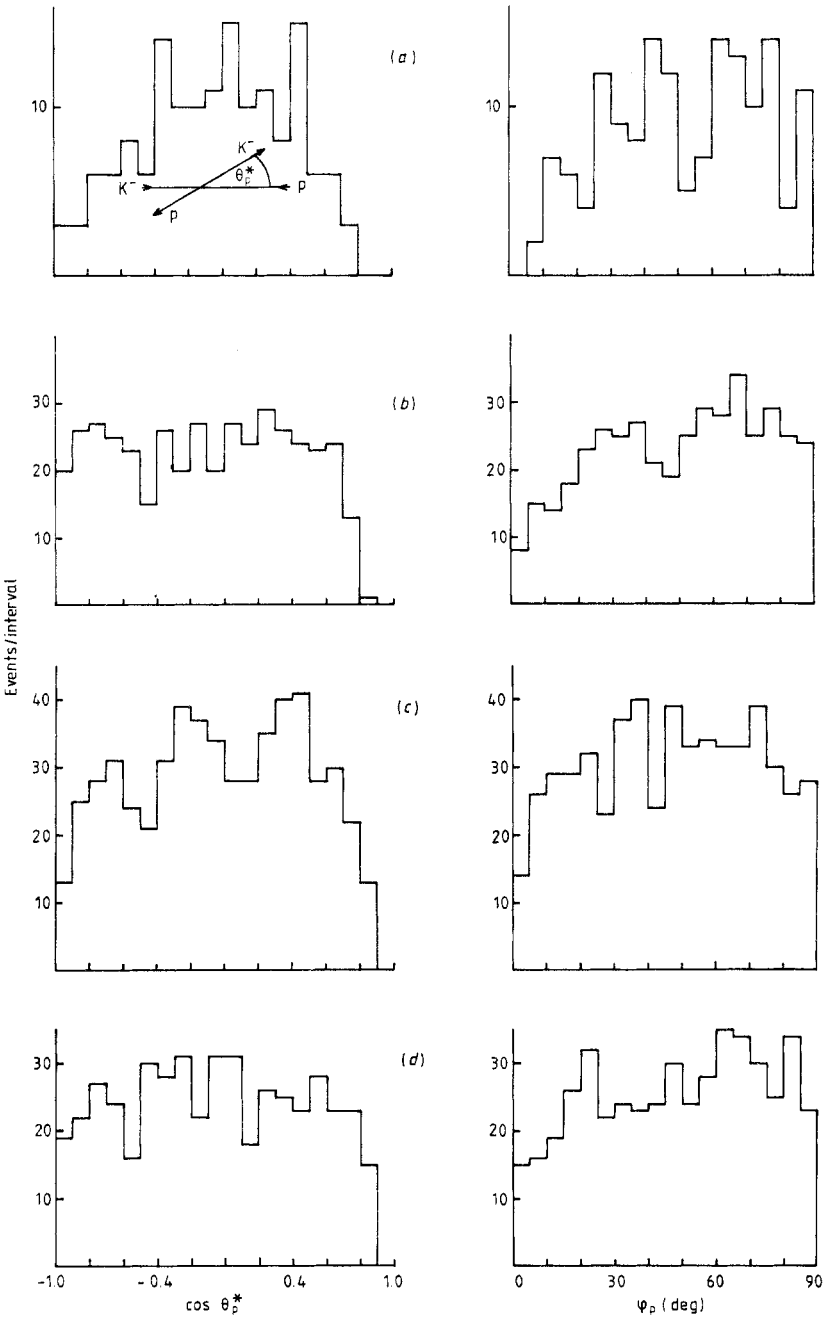

Figure 2. Production angular distributions for elastic scattering. Some loss of events is apparent at $\cos\theta_p^* \sim \pm 1$ and $\varphi_p \lesssim 20°$. (*a*) $110 \leqslant p_{K^-} < 150$ MeV/*c*; (*b*) $150 \leqslant p_{K^-} < 190$ MeV/*c*; (*c*) $190 \leqslant p_{K^-} < 230$ MeV/*c*; (*d*) $230 \leqslant p_{K^-} < 300$ MeV/*c*.

Table 1.

K^- momentum (MeV/c)	$\cos\theta_p^*$	φ_p (deg)	Number of events after cuts	Scaling weight
110–150	−0.6→0.5	25–90	101	2.52
150–190	−0.9→0.7	20–90	334	1.61
190–230	−0.9→0.7	15–90	435	1.50
230–290	−0.9→0.8	15–90	372	1.41

weights are given in table 1. After these cuts have been made no correlation is observed between φ_p and $\cos\theta_p^*$.

The total weight to correct for losses is given by

$$W = W_s W_e W_m$$

where W_s is the scaling weight, $W_e(=1.007)$ is the weight for scanning efficiency and $W_m(=1.077)$ is the weight for measuring efficiency.

Unfitted events were distributed into momentum intervals according to their measured momenta; their distributions of $\cos\theta_p^*$ and φ_p were assumed to be the same as for the fitted events. With the above weighting and the total path length of kaons determined from one-prong decays the cross sections for elastic scattering have been determined and are shown in table 2 together with the plotting momentum and its dispersion. No cross sections are given below 150 MeV/c since the loss of events (see table 1) due to short tracks is severe, the weighting is large and the correction uncertain. The cross sections are shown in figure 3 as a function of momentum where they are compared with Kim's (1966) values and those of Mast *et al* (1976b). Not shown are the results of Sakitt *et al* (1965) which are similar to those of Kim (1966). Agreement is good.

4. Charge-exchange scattering

Close to the threshold for charge exchange the momenta of the neutral kaons produced are modest relative to the centre-of-mass momenta of the pions from K_s^0 decay. Consequently, the laboratory angle between the two pion tracks is close to 180° and the decay vertex may resemble a kinked track rather than a V^0. At scanning such decays may easily be

Table 2.

Momentum interval MeV/c)	Number of events after cuts	Corrected number of events	Path length (m)	Cross section (mb)	Plotting momentum (MeV/c)	Dispersion (MeV/c)
150–170	175	305 ± 23	1018 ± 55	88 ± 8	163	23
170–190	206	360 ± 25	1464 ± 76	72 ± 6	182	20
190–210	221	360 ± 24	1958 ± 88	54 ± 4	199	17
210–230	252	410 ± 26	2173 ± 92	55 ± 4	218	17
230–250	215	329 ± 23	1809 ± 92	53 ± 5	234	15
250–270	128	196 ± 17	1187 ± 96	48 ± 6	249	16
270–290	52	79 ± 11	590 ± 89	39 ± 9	267	29

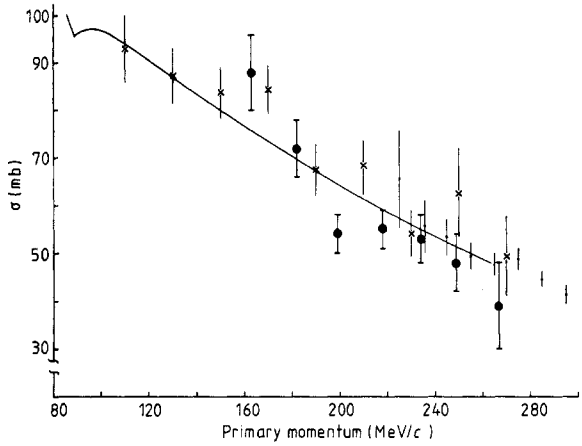

Figure 3. Cross sections for $K^-p \to K^-p$ elastic scattering compared with earlier data. The curve is obtained from Martin's (1981) analysis of kaon data using forward dispersion relations. ●, this experiment; ×, Kim (1966); ·, Mast *et al* (1976b).

overlooked and cuts have had to be imposed to allow for losses due to this effect.

A total of 507 charge-exchange scatterings were recorded of which 485 were measured. The selection on vertex coordinates left a final sample of 448 events for further analysis, of which 392 gave an overall fit to reaction (2).

For the fully fitted events, by considering the variation of mean lifetime with r_s and also the production and decay angular distributions, the selection criteria of table 3 were chosen. For unfitted events GEOMETRY values were used and the criteria of table 3 applied. The few unmeasured events were examined on the scanning table and a judgement made. The total weight to correct for all losses is

$$W = 1.67 W_r W_e W_n.$$

Here W_r is the weight for the loss of events outside the allowed range of r_s and outside the fiducial volume. This weight is momentum dependent and on average is of the order of 1.2. The scanning efficiency weighting, W_e, is 1.05 and the weighting for K^0_L and neutral decays W_n, is 2.92.

The corrected distribution of $\cos\theta^*_p$ is shown in figure 4. There is no convincing evidence for P waves. Finally the cross sections are determined as a function of momentum

Table 3. K^- momentum: 90–290 MeV/*c*.

		Events after cuts
r_s	$0.06 < r_s < 3.0$ cm	370
φ_d	$30 < \varphi_d < 90°$	285
$\cos\theta^*_d$	$-1.0 < \cos\theta^*_d < 0.8$	269
φ_p, $\cos\theta^*_p$	no cut applied	269
Scaling weight, W_s	$1.67 W_r$	

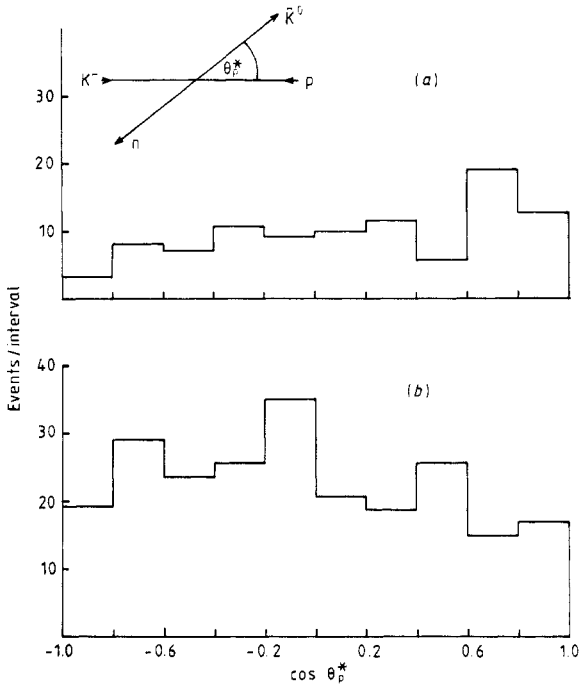

Figure 4. Production angular distributions for charge exchange. (*a*) 90–170 MeV/*c*; (*b*) 170–300 MeV/*c*.

and these are given in table 4 and are shown in figure 5. Compared with the cross sections obtained by Kim (1966) there is a considerable discrepancy: the new cross sections are some 60% larger. The consequences of this are discussed later.

5. The channels $K^-p \to \pi^\pm \Sigma^\mp$ in flight

The in-flight production of $\Sigma^\pm$ hyperons followed by decay gives rise to the numbers of

Table 4.

Primary momentum MeV/*c*	Number of events after cuts	Corrected number of events	Track length (m)	Cross section (mb)	Plotting momentum (MeV/*c*)	Dispersion (MeV/*c*)
90–130†	36	229 ± 38	1431 ± 28	47 ± 8	110	—
130–170†	36	240 ± 39	2802 ± 56	25 ± 4	150	—
170–210	96	579 ± 57	9712 ± 788	17 ± 2	191	20
210–250	86	570 ± 56	10681 ± 890	16 ± 2	226	18
250–290	27	161 ± 31	6704 ± 1196	7 ± 2	256	24

† Cross sections at these momenta have been determined using the WHS condition. This leads to a small change in the total numbers of events as compared with table 3.

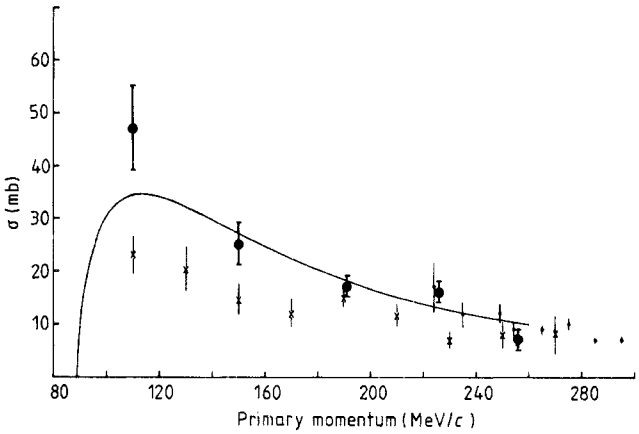

Figure 5. Cross sections for charge-exchange scattering. ●, this experiment; ×, Kim (1966); ·, Mast *et al* (1976b); ——, Martin (1981).

events classified below:

$$990\ \Sigma_p^+ \text{ events:} \qquad K^-p \to \pi^-\Sigma^+ \qquad \Sigma^+ \to \pi^0 p \tag{3.1}$$

$$1052\ \Sigma_\pi^+ \text{ events:} \qquad K^-p \to \pi^-\Sigma^+ \qquad \Sigma^+ \to \pi^+ n \tag{3.2}$$

$$2364\ \Sigma_\pi^- \text{ events:} \qquad K^-p \to \pi^+\Sigma^- \qquad \Sigma^- \to \pi^- n. \tag{4.1}$$

A smaller number of the Σ hyperons produced interact. These are almost entirely Σ^- absorptions at rest:

$$356\ \Sigma_\sigma \text{ events:} \qquad K^-p \to \pi^+\Sigma^- \qquad \Sigma^-p \to \Lambda^0 n \text{ or } \Sigma^0 n. \tag{4.2}$$

In-flight events are defined by the lack of collinearity of the tracks of their secondary particles. In an additional sample of events with unresolved production and decay vertices the following event classes are distinguished where the events are judged by template to be in flight with kaon momentum in excess of 140 MeV/c:

$$234\ \pi^-p \text{ events:} \qquad K^-p \to \pi^-(\Sigma^+) \qquad (\Sigma^+) \to \pi^0 p$$

$$476\ \pi^-\pi^+ \text{ events:} \qquad K^-p \to \pi^\mp(\Sigma^\pm) \qquad (\Sigma^\pm) \to \pi^\pm n$$

where the brackets indicate an unseen hyperon. The above number of π^-p events does not contain short-lived Λ hyperons. These have been recognised by measuring the momentum of the pion. After removing the Λ hyperon decays the remainder of the events correspond largely to either Σ_p^+ hyperons produced backwards in the CM (very slow in the laboratory frame) or Σ_p^+ events where the Σ^+ hyperon and proton tracks are nearly collinear. The above sample of $\pi^+\pi^-$ events is contaminated from very short-lived $\bar{K}^0$ decays (~15%) and by $\Lambda\pi\pi$ production (~3%). Moreover, since the momentum of the production pion is very similar to that of the decay pion (~200 MeV/c) there is almost complete kinematic overlap between Σ_π^+ and Σ_π^- event categories. The cuts are devised so that both classes of unresolved events are not used in the analysis.

In preparing the final sample, events with $r_s < 1$ mm have been cut and weights calculated in the same manner as for the charge-exchange channel. After this selection the angular distributions of production and decay were examined for losses and cuts were imposed as given in table 5. The distributions of φ_p, $\cos\theta_d^*$ and φ_d appear to be isotropic

Table 5.

	Σ_p^+	Events after cuts	Σ_π^+	Events after cuts	Σ^-	Events after cuts
r_Σ	> 1 mm	724	> 1 mm	786	> 1 mm	1978
φ_p	0→90	724	0→90	786	10→90	1826
φ_d	15→90	639	0→90	786	0→90	1826
$\cos\theta_d^*$	−1.0→0.8	594	−1.0→1.0	786	−1.0→1.0	1826
$\cos\theta_p^*$	−0.9→0.9	567	−0.9→0.9	752	−0.9→0.8	1659
Scaling weight	$1.48W_r$	—	$1.11W_r$	—	$1.32W_r$	—

for the angular regions given in table 5 and the distribution of $\cos\theta_p^*$ is flat or linear in $\cos\theta_p^*$ depending upon the primary momenta which are all in the region 90–300 MeV/c. Note that those events where the Σ hyperon track is close to the line of the beam track are eliminated by the cut on $\cos\theta_p^*$. Such events may not be recognised as non-collinear events. Consequently, apart from the $\cos\theta_p^*$ distribution, simple scaling outside the selected region is sufficient to correct for losses.

5.1. *Angular distributions and polarisation in $\Sigma^\pm$ hyperon production*

The production angular distributions weighted for the cut $r_s < 1$ mm are shown in figure 6. The departure from isotropy implies the presence of partial waves other than S waves and

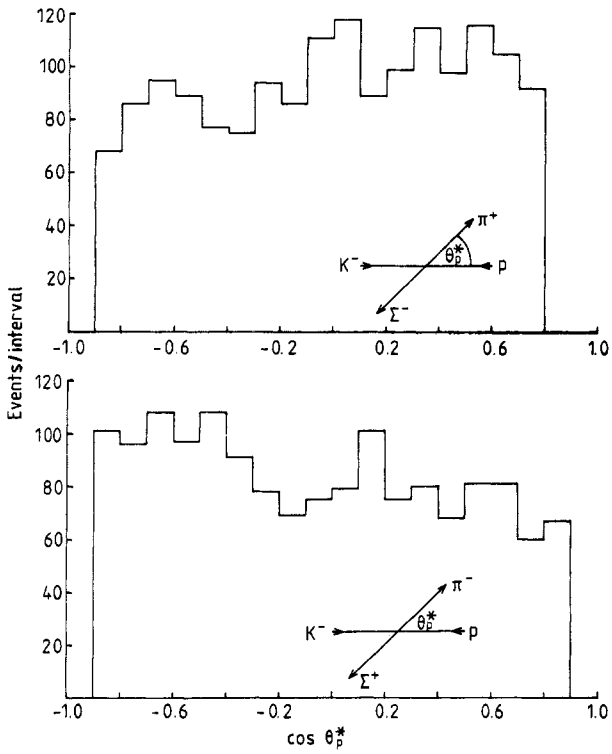

Figure 6. Production angular distributions of charged Σ hyperons.

Table 6.

p_{K^-} (MeV/c)		90–150	150–190	190–230	230–300	Total
Average p_{K^-} (MeV/c)		125	171	209	252	—
A_1/A_0	Σ^+	-0.20 ± 0.15	-0.41 ± 0.11	-0.26 ± 0.09	-0.12 ± 0.12	-0.27 ± 0.06
	Σ^-	0.01 ± 0.10	0.32 ± 0.10	0.22 ± 0.11	0.15 ± 0.14	0.20 ± 0.05

it is of great interest to determine experimentally where they begin to contribute. The data of figure 6 have been separated into four intervals of primary momentum and a satisfactory fit to the production angular distributions over the unbiased region of $\cos\theta_p^*$ was found with

$$dN/d(\cos\theta_p^*) \propto (1 + A_1/A_0 P_1(\cos\theta_p^*))$$

where contributions from higher partial waves were found to be unnecessary. The results of the fit are shown in table 6. They are displayed in figure 7 where they compare well with the values of Bangerter *et al* (1981).

The production of charged hyperons in the primary momentum interval (90–150 MeV/c) is consistent with isotropy and hence solely S waves. However, departure from isotropy is apparent in the higher momentum intervals with P waves evidently setting in. If P waves are present then the polarisation of the Σ^+ hyperon might be seen from the interference of the S and P waves. This should be apparent as a lack of symmetry of the angle of emission, β, of the proton in $\Sigma^+ \to p\pi^0$ relative to the normal to the production plane†. The experimental distribution of this angle is shown in figure 8. It is linear in $\cos\beta$ which is consistent with the decay of polarised hyperons. The up/down asymmetry $(U-D)/(U+D)$ of the decay proton relative to the production plane can be used to determine the average polarisation of the Σ^+ hyperon. Allowing for the cuts applied to the data at the decay vertex

$$(U-D)/(U+D) = 0.527\alpha\langle P\rangle$$

where $\alpha = -0.979$ for Σ_p^+ decays and $\langle P\rangle$ is the average polarisation for the selected interval $-0.9 < \cos\theta_p^* < 0.9$. It is found that the average polarisation for the first interval, 90–150 MeV/c, is zero as expected since the production angular distributions of the Σ^+ and Σ^- hyperons are isotropic in this interval indicating the absence of P waves. For momenta above about 150 MeV/c polarisation might be expected. Confining the analysis to this region the average polarisation is given by

$$\alpha\langle P\rangle = -0.27 \pm 0.08.$$

The values for individual momentum bins are shown in table 7.

In order to compare the polarisation with that obtained by Bangerter *et al* (1981) it is necessary to re-express the joint production and decay distribution in terms of polarisation coefficients B_l. When the highest value of l is 1 then

$$\frac{d^2N}{d\cos\theta_p^*\, d\cos\beta} \propto \left(1 + \frac{A_1}{A_0} P_1(\cos\theta_p^*) + \cos\beta \frac{B_1}{A_0} P_1^1(\cos\theta_p^*)\right)$$

† β is defined by $\cos\beta = [(\boldsymbol{K}\times\boldsymbol{\Sigma})\cdot\boldsymbol{P}]/|\boldsymbol{K}\times\boldsymbol{\Sigma}|\,|\boldsymbol{P}|$ in the left-handed system of coordinates of the TST chamber. Here $\boldsymbol{K}$, $\boldsymbol{\Sigma}$ and $\boldsymbol{P}$ are the directions of the kaon, the hyperon and the proton in the Σ^+ CM frame. This definition is equivalent to that of Bangerter *et al* (1981).

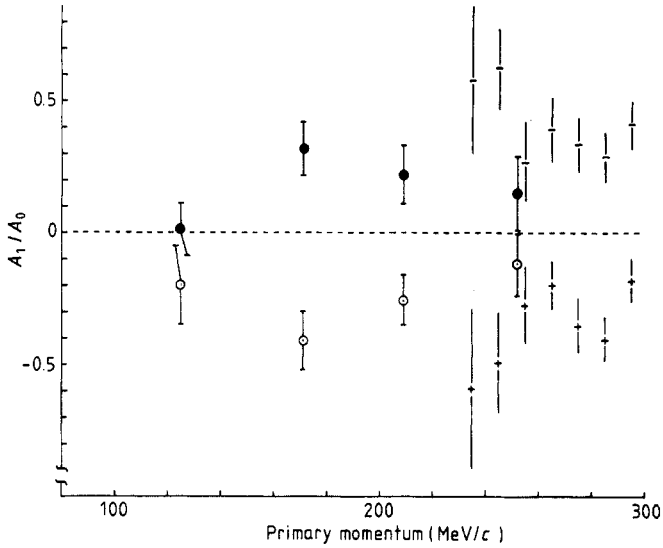

Figure 7. Variation of A_1/A_0 with primary momentum for charged Σ hyperon production. This experiment: ●, Σ^-; ○, Σ^+. Bangerter *et al* (1981): −, Σ^-; +, Σ^+.

where, in the nomenclature of Bangerter *et al*, α is absorbed into B_1. Then over the interval of $\cos\theta_p^*$ that has been used

$$B_1/A_0 = 1.19\alpha\langle P\rangle.$$

The values of B_1 for the present data are given in table 7 and are shown in figure 9 along with those of Bangerter *et al* (1981). There is reasonable agreement and the new data are consistent with an extrapolation of the data of Bangerter *et al* down to lower momenta.

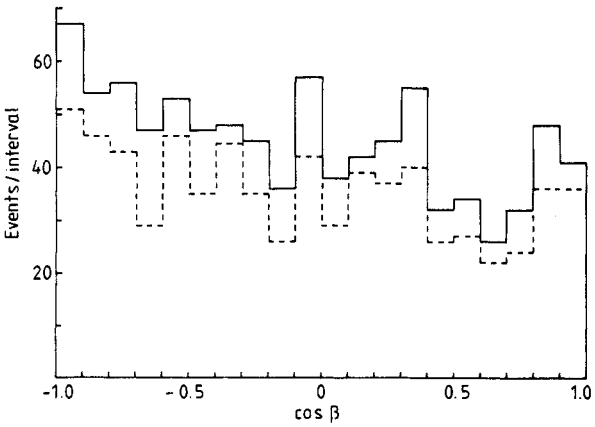

Figure 8. Distribution of the angle between the direction of the decay proton and the normal to the production plane of the Σ^+ hyperon. Full curve, $r_s > 1$ mm; broken curve, selections of table 5.

Table 7.

p_{K^-} [MeV/c]	Average p_{K^-} [MeV/c]	U	D	$\alpha\langle P\rangle$	B_1/A_0
90–150	125	52 ± 8	55 ± 9	-0.049 ± 0.212	-0.058 ± 0.252
150–190	171	88 ± 10	122 ± 12	-0.303 ± 0.145	-0.361 ± 0.173
190–230	209	99 ± 11	128 ± 13	-0.247 ± 0.140	-0.294 ± 0.167
230–300	252	79 ± 10	103 ± 11	-0.248 ± 0.154	-0.295 ± 0.183

5.2. Cross sections for $\Sigma^\pm$ hyperon production

After correction for the selections described above and from the fit to the anisotropic production angular distributions, the initial and corrected numbers of $\Sigma^\pm$ hyperon events are given in table 8. The track lengths and corresponding cross sections and their ratios $\gamma\,(=\Sigma^-/\Sigma^+)$ are also given. A check on the quality of the corrected data has been made by examining the two ratios $B=\Sigma_\pi^+/(\Sigma_\pi^+ + \Sigma_p^+)$ and γ. For events satisfying the selection criteria of table 5, and corrected by weighting, the value of B is 0.493 ± 0.027. The world average (Particle Data Group 1980) of B is 0.484 ± 0.003. The values of γ above 170 MeV/c primary kaon momentum have also been determined by a method similar to that used earlier by this collaboration (Nowak *et al* 1978). The method does not involve cuts and consequent weighting. In fact it uses all the events found in scanning including the unresolved π^-p and $\pi^-\pi^+$ events. The two sets of γ values so obtained, while not completely independent, are in good agreement. The consistency of the B and γ ratios confirms the validity of the selections and weightings used.

The cross sections from table 8 are displayed in figures 10(*a*) and (*b*). The normalisation for the first four momentum intervals is determined from events whose primaries have stopped or would have stopped in the fiducial volume; the normalisation for the remaining intervals is determined from one-prong decays. In the overlap region where

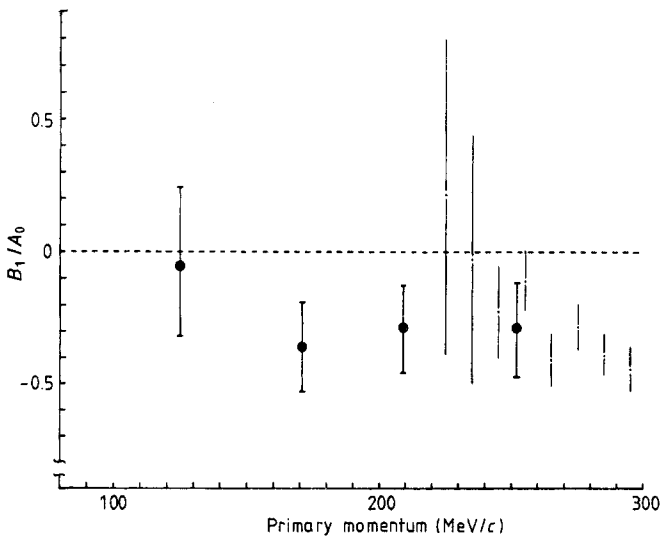

Figure 9. Variation of the polarisation coefficient B_1/A_0 with primary momentum. ●, this experiment; •, Bangerter *et al* (1981).

Table 8.

p_{K^-} (MeV/c)	Observed number of events after cuts			Corrected number of events			$\gamma=\Sigma^-/\Sigma^+$	Track length (m)	Cross section (mb)		Plotting momentum (MeV/c)	Dispersion (MeV/c)	$\gamma=\Sigma^-/\Sigma^+$
	Σ_p^+	Σ_π^+	Σ^-	Σ_p^+	Σ_π^+	Σ^-			Σ^+	Σ^-			
90–110†	14	26	81	27 ± 7	37 ± 7	129 ± 15	2.02 ± 0.39	559 ± 12	34 ± 5	68 ± 8	100	—	—
110–130†	15	27	116	30 ± 8	39 ± 7	179 ± 17	2.59 ± 0.47	875 ± 17	23 ± 4	60 ± 6	120	—	—
130–150†	31	37	128	60 ± 11	51 ± 8	193 ± 17	1.74 ± 0.26	1237 ± 24	26 ± 3	46 ± 4	140	—	—
150–170†	37	47	110	69 ± 11	65 ± 10	164 ± 16	1.22 ± 0.18	1571 ± 31	25 ± 3	31 ± 3	160	—	1.30 ± 0.16
170–190	94	94	216	173 ± 18	129 ± 13	341 ± 24	1.13 ± 0.11	4212 ± 249	21 ± 2	24 ± 2	182	20	0.95 ± 0.12
190–210	104	149	233	193 ± 19	206 ± 17	377 ± 28	0.94 ± 0.09	5500 ± 305	21 ± 2	20 ± 2	199	17	1.05 ± 0.13
210–230	83	124	168	153 ± 17	172 ± 16	254 ± 20	0.78 ± 0.08	5891 ± 329	16 ± 1	13 ± 1	218	17	0.96 ± 0.13
230–250	60	77	130	107 ± 14	108 ± 12	196 ± 17	0.91 ± 0.11	4790 ± 296	13 ± 1	12 ± 1	234	15	0.90 ± 0.15
250–270	36	51	79	65 ± 11	71 ± 10	123 ± 14	0.90 ± 0.14	3604 ± 256	11 ± 1	10 ± 1	249	16	1.08 ± 0.22
270–290	30	22	36	53 ± 10	31 ± 6	59 ± 12	0.70 ± 0.17	1838 ± 180	13 ± 2	9 ± 2	267	29	—

† Cross sections at these momenta were determined using the WHS normalisation.

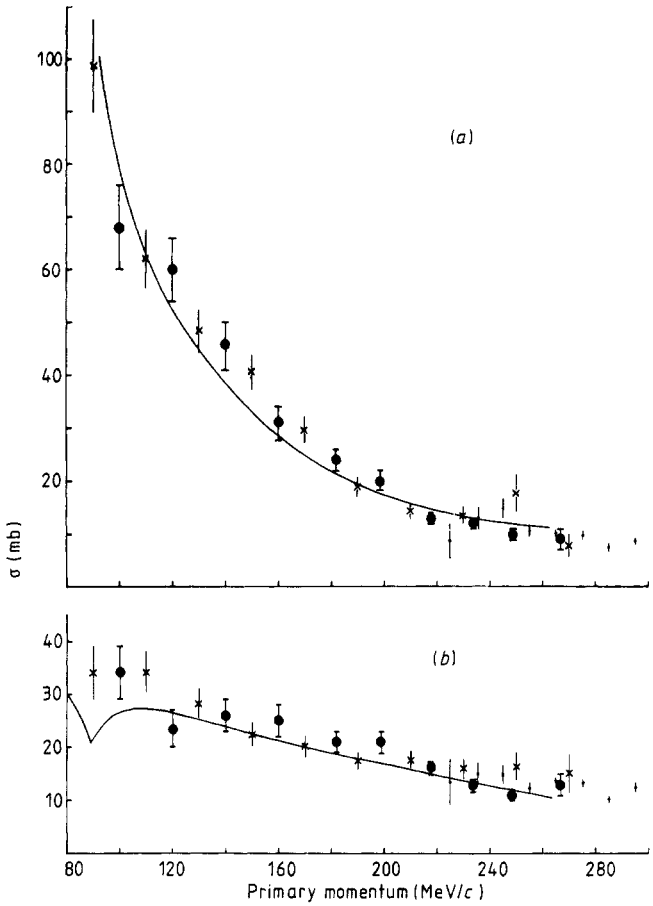

Figure 10. Cross sections for charged hyperon production (*a*) $K^-p \rightarrow \pi^+\Sigma^-$; (*b*) $K^-p \rightarrow \pi^-\Sigma^+$. ●, this experiment; ×, Kim (1966); •, Bangerter *et al* (1981); ——, Martin (1981).

both normalisations are appropriate the resulting values of cross sections are in excellent agreement. Also shown on the figures are the cross sections obtained by Kim (1966) and Bangerter *et al* (1981). There is good agreement between the cross section values and also with those, not shown, of Sakitt *et al* (1965).

6. Discussion

In figures 3, 5 and 10 the cross sections determined above are compared with those of Kim (1966) and with those of the LBL group (Mast *et al* 1968, 1973a, b, 1976a, b, Bangerter *et al* 1981) where there is an overlap of primary momenta. There is good agreement with the results of LBL at these higher momenta. In the comparison with the data of Kim (1966) there is good correspondence between the cross sections for elastic scattering and charged Σ production. This implies that normalisation is not responsible for the discrepancy between the charge-exchange cross sections. The smallest possible cross sections for charge-exchange scattering can be calculated from the observed numbers of events if corrected only for resolution and scanning loss with the incorrect assumption that all

events are equally observable. Such corrections do not allow for the more subtle geometrical biases which have been shown on detailed examination to be present. These minimum cross sections are at least equal to Kim's corrected values, whereas when cuts and corrections have been made, the resulting cross sections, averaged over the momentum interval 90–290 MeV/c, are about 1.6 times larger than the values of Kim (1966). Work is in progress to redetermine these discrepant cross sections with larger statistics. One effect of the enhanced cross section will be to raise the value of the isospin-one scattering length. A preliminary analysis indicates this but confirmation must await the completion of our other TST data.

The nature of the losses in the elastic scattering channel and the small number of charge-exchange events prevent a detailed analysis of the contribution of P waves at these low momenta. However, there is a clear indication from the angular distributions of the production of charged hyperons that significant P waves are involved at primary momenta which are lower than previously observed. This result is supported by the finite polarisation of the Σ^+ hyperons seen from their decays into protons. These have implications concerning the validity of purely S-wave analyses.

Acknowledgments

We wish to thank our respective scanning staffs and that of the Rutherford Laboratory for their careful work in a difficult experiment, and the crews of the extinct NIMROD machine at the Rutherford Laboratory for making the exposures possible. Thanks are due to Professor A D Martin for discussions and his ever available advice. Finally we should like to thank the Science Research Council for its support.

Appendix. Path length normalisation for cross sections

A.1. Normalisation from observed K^--meson decays; one-prong method suitable for 150 MeV/c and above

The standard method of determining the flux in a kaon experiment has always been to measure a sample of $K^{\mp} \to \pi^+\pi^-\pi^{\mp}$ decays. The four-constraint fit on each event gives an accurate value for the kaon momentum and the distribution of these momenta can be converted into a total path length distribution through the known mean-free-path for decay. But in the 90–300 MeV/c region there are far more K^--meson interactions than there are three-pion decays so it is necessary to use one-prong decays to give sufficient statistics for the normalisation. The channels with one track or 'prong' are found with high efficiency at these low momenta (as distinct from high momenta) since the angles of decay are large in the laboratory frame and there is usually a distinctive change in ionisation between the primary and the decay secondary track. The one-prong channels include $K^- \to \mu^-\bar{\nu}$, $K^- \to \pi^-\pi^0$, $K^- \to \mu^-\pi^0\bar{\nu}$, $K^- \to e^-\pi^0\bar{\nu}$ and $K^- \to \pi^-\pi^0\pi^0$. They cannot be clearly separated from one another by kinematic fitting and the fit makes little or no improvement to the measured momentum of the incident kaon. Below 150 MeV/c the number of decays is small and the momenta are badly determined so that a completely different technique of normalisation is preferred (see § A.2 below). The path length, ΔL, for the kaons of mass m and lifetime τ traversing a given momentum interval Δp can be

expressed in the following form

$$\Delta L = \frac{c\tau}{Bm} \sum_i p_i \tag{A.1}$$

where p_i denotes the decaying kaon momentum and the sum is extended over all the events found in that interval; B is the branching ratio of the one-prong mode. Using $\bar{p} = \Sigma p_i / N_d$, where N_d is the total number of decay events, the cross section, σ, is given by

$$\sigma = \frac{m}{c\tau n} \frac{1}{p} \frac{N_i}{N_d} \tag{A.2}$$

where N_i is the number of events in the interaction channel of interest and n is the number of scattering centres per unit volume. Direct use of (A.2) requires care. Since the empirical value of N_d is taken from the unfitted momentum distribution the value of N_i should be related to the same interval of unfitted momentum and not to fitted momentum, otherwise distortions would arise owing to the difference in the errors on the fitted and unfitted momenta (Fallahi 1977, Hamam 1978). But this procedure could lead to the calculation of a cross section at a momentum where there are actually no events whatsoever, the apparent events having come from the spread induced by measurements.

Ideally the resolution function would be known and a full deconvolution carried out, but the situation can be improved if the cross section obtained from expression (A.2) is referred to a 'plotting momentum'. Strictly, the momentum to which the cross section applies is the average of the momenta of *all* beam particles in the interval Δp. However, provided Δp is small enough, and there are no violent changes in the slope of the cross section with momentum, the average momentum found from the decays will be very close to this value. For each interval of measured momentum the average value, $\bar{p}$, comes from the fitted kaon momenta for the four-constraint $K^- \to \pi^- \pi^- \pi^+$ events in that measured interval. The typical error on these fitted momenta is much smaller than the width of the momentum intervals into which the data have been divided. This is the correct average momentum required to calculate the path length (see (A.1) and (A.2) above); it is also the best estimate we have of the beam momentum appropriate to the cross section that is determined. Therefore it has been used as the plotting momentum for the cross section from expression (A.2).

For intervals close to the central momentum range (from ~180 to ~230 MeV/c) the shift from a mean measured momentum to a plotting momentum is negligible. On the wings where the distributions are falling off rapidly the value of the plotting momentum may even lie outside the measured-momentum interval from which it is derived.

As well as the plotting momentum the tables of cross sections list a 'dispersion' for each measured momentum interval. This is just the root-mean-square deviation about the plotting momentum for the four-constraint fitted kaon momenta from $K^- \to \pi^- \pi^- \pi^+$ events in that interval. It gives a measure of the smearing between adjacent points on the graphs of cross sections. The track lengths quoted in tables 2, 4 and 8 are derived from the product of plotting momentum and the number of one-prong events in a given interval.

A.2. Normalisation from stopped K^--meson interactions; WHS method, suitable for below 170 MeV/c

A large majority of the K^- mesons which slow down to below 170 MeV/c come to rest in the hydrogen and interact. Many of these interactions give rise to collinear $\Sigma^+ \pi^-$ or $\Sigma^- \pi^+$

final states which can be clearly recognised. The total number of stopping kaons is calculated by correcting for those which produce neutral hyperons, using our earlier results (Kumar 1981).

The total number of kaons passing through a momentum p is given by

$$N(p) = N_i(p) + N_d(p) \tag{A.3}$$

where $N_i(p)$ is the number which interact at a momentum less than p and $N_d(p)$ is the number decaying at less than p. At the lowest momenta only a small fraction of the kaons decay and their momenta are badly measured so it is more convenient to eliminate $N_d(p)$ by use of the decay law and write

$$N(p) = N_i(p) - \frac{m}{c\tau}\int_0^p p^{-1}N(p)\frac{dx}{dp}\,dp \tag{A.4}$$

where dx/dp is given by the rate of energy loss in the liquid. By far the largest contribution to (A.4) comes from the number of kaons which interact at rest. Their momenta are precisely known. Events which are observed to interact in flight are included at their fitted momenta. There is now no serious problem due to measurement errors. Equation (A.4) is easily solved for $N(p)$ and track lengths can then be calculated by multiplying by dx/dp and intergrating over the required momentum interval.

It is only possible to use these track lengths to compute the cross sections for interactions of beam particles which would have stopped in the TST. Higher-momentum particles or those few with large dip angles do not contribute to the sample of $\Sigma\pi$ events produced by K^--meson interactions at rest. That is why this 'would have stopped' (WHS) method is only useful for calculating cross sections below about 170 MeV/c. Above this the one-prong normalisation makes use of the whole sample of interactions while the WHS method is forced to discard many events.

In the region from 150 to 170 MeV/c where both methods are valid the cross sections obtained by the two techniques are in excellent agreement.

References

Abrams G S and Sechi-Zorn B 1965 *Phys. Rev.* **139** B454

Bangerter R O, Alston-Garnjost M, Barbaro-Galtieri A, Mast T S, Solmitz F T and Tripp R D 1981 *Phys. Rev.* D **23** 1484

Batty C J 1980 *Nukleonika* **25** 545

Chao Y A and Kraemer R W 1973 *Nucl. Phys.* B **56** 46

Dalitz R H and McGinley J G 1981 *Low and Intermediate Energy Kaon–Nucleon Physics* ed E Ferrari and G Violini (Dordrecht: Reidel) p 381

Davis D H, Tovee D N and Nowak R 1977 *Nukleonika* **22** 845

Fallahi M T 1977 *Thesis* University of Durham

Goossens M, Wilquet G, Armstrong J L and Bartley J H 1981 *Low and Intermediate Energy Kaon–Nucleon Physics* ed E Ferrari and G Violini (Dordrecht: Reidel) p 243

Hamam Y A 1978 *Thesis* University of Durham

Henley E M, Alberg M A and Wilets L 1980 *Nukleonika* **25** 567

Humphrey W E and Ross R R 1962 *Phys. Rev.* **127** 1305

Kim J K 1965 *Phys. Rev. Lett.* **14** 29

—— 1966 *Columbia University Report No Nevis 149*

—— 1967 *Phys. Rev. Lett.* **19** 1074

Kittel W, Otter G and Wacek I 1977 *Phys. Lett.* **21** 349

Kumar K S 1981 *Low and Intermediate Energy Kaon–Nucleon Physics* ed E Ferrari and G Violini (Dordrecht: Reidel) p 259

Martin A D 1981 *Low and Intermediate Energy Kaon–Nucleon Physics* ed E Ferrari and G Violini (Dordrecht: Reidel) p 97
Mast T S, Alston-Garnjost M, Bangerter R O, Barbaro-Galtieri A S, Gershwin L K, Solmitz F T and Tripp R D 1968 *Phys. Rev. Lett.* **21** 1715
Mast T S, Alston-Garnjost M, Bangerter R O, Barbaro-Galtieri A S, Solmitz F T and Tripp R D 1973a *Phys. Rev.* D **7** 5
—— 1976a *Phys. Rev.* D **11** 3078
—— 1976b *Phys. Rev.* D **14** 13
Mast T S, Bangerter R O, Alston-Garnjost M, Barbaro-Galtieri A S, Gershwin L K, Solmitz F T and Tripp R D 1973b *Phys. Rev.* D **7** 3212
Miller D J 1980 *Nukleonika* **25** 497
Nordin P 1961 *Phys. Rev.* **123** 2168
Nowak R J *et al* 1978 *Nucl. Phys.* B **139** 61
Particle Data Group 1980 *Rev. Mod. Phys.* **52** 1
Sakitt M, Day T B, Glasser R G and Seeman N 1965 *Phys. Rev.* **139** B719
Schlosser K, Buschbeck-Czapp B, Hromadmik H and Otter G 1965 *Phys. Lett.* **17** 334
Watson M B, Ferro-Luzzi M and Tripp R O 1963 *Phys. Rev.* **131** 2248